axioms

MDPI

Article

Steam Gasification in a Fluidized Bed with Various Methods of In-Core Coal Treatment

Nikolay Abaimov [1,*], Alexander Ryzhkov [1], Vladimir Tuponogov [1], Leonid Simbiriatin [2], Alexey Dubinin [1], Lu Ding [3] and Sergey Alekseenko [1,4]

[1] Ural Power Engineering Institute, Ural Federal University Named after the First President of Russia B.N. Yeltsin, Str. Mira, 19, 620002 Yekaterinburg, Russia; a.f.ryzhkov@urfu.ru (A.R.); v.g.tuponogov@urfu.ru (V.T.); a.m.dubinin@urfu.ru (A.D.); aleks@itp.nsc.ru (S.A.)
[2] "Promyshlennyj Perlit", 4b/35 V. Vysotsky Street, 620072 Yekaterinburg, Russia; leonid.simbiryatin@gmail.com
[3] Key Laboratory of Coal Gasification and Energy Chemical Engineering of the Ministry of Education, East China University of Science and Technology, Shanghai 200237, China; dinglu101@163.com
[4] Kutateladze Institute of Thermophysics SB RAS, 1 Academician Lavrentiev Avenue, 630090 Novosibirsk, Russia
* Correspondence: nick.sum41@mail.ru; Tel.: +7-906-815-08-28

Abstract: The aim of this work is to study coal steam gasification with various methods of coal in-core treatment in FB using a newly developed thermodynamic calculation method. A calculational study of subbituminous coal steam non-catalytic gasification was carried out using four different methods of coal in-core treatment in single-vessel multisectional fluidized-bed gasifiers. A semi-empirical model based on the entropy maximization thermodynamic method and "restricted equilibria" based on previously obtained experimental data has been developed. Based on thermodynamic calculations, the effect of the leading thermochemical processes and operating parameters of the fluidized bed (temperature, fluidization number, steam/coal ratio feed rate) was revealed. New information was obtained regarding the composition of char and syngas at the gasifier outlet, the syngas heating value, and the cold gas efficiency of the steam gasification of Borodinskiy subbituminous coal char. The results indicate the possibility of significantly accelerating and improving non-catalytic steam gasification in fluidized bed gasifiers through the appropriate organization of in-core coal treatment. Based on the results obtained, the following recommendation is made—when designing multi-section and multi-vessel steam-blown gasifiers, the ratio of residence times should be set in favor of increasing the coal residence time in the steam-blown carbonization zone. Structurally, this can be achieved by increasing the volume and/or area of the steam-blown carbonization section (vessel).

Keywords: engineering calculations; mathematical modeling; improvement of technical devices; coal; syngas; steam gasification; bubbling fluidized bed; thermodynamic

MSC: 74A15; 81T80; 62P30

check for updates

Citation: Abaimov, N.; Ryzhkov, A.; Tuponogov, V.; Simbiriatin, L.; Dubinin, A.; Ding, L.; Alekseenko, S. Steam Gasification in a Fluidized Bed with Various Methods of In-Core Coal Treatment. *Axioms* **2023**, *12*, 587. https://doi.org/10.3390/axioms12060587

Academic Editor: Leonid Plotnikov

Received: 4 May 2023
Revised: 10 June 2023
Accepted: 11 June 2023
Published: 13 June 2023

1. Introduction

Steam gasification in a fluidized bed (FB) is, theoretically, an ideal way to produce high-quality, medium heating value syngas for energy and chemical technologies in a non-catalytic low-temperature process that ensures the unit's slag-free operation at a satisfactory conversion rate [1].

Steam gasification in FB was initially developed in the 1970s with the aim of obtaining medium heating value syngas from coal (about 10 MJ/m^3) for a high-capacity integrated gasification combined cycle (IGCC) and as a feedstock for large chemical enterprises. The process, in accordance with technological requirements, was carried out, as a rule, under a pressure of up to 4 MPa in the low temperature range of 650–1100 °C [2]. Recently, steam gasification in a bubbling FB (BFB) has gained renewed popularity with the development of distributed generation on a local raw fuel base (low-grade coals and biomass), which needs highly efficient energy and chemical sources of low-pressure syngas. Interest in coal is present both in emerging [3–5] and developed economies [1,6–8].

One direction in the modern transition to alternative energy sources is the use of hydrogen, which can be obtained in its pure form from solid fuel syngas [5,9]. Syngas with a high hydrogen content is also used in power plants with solid oxide fuel cells [10].

A characteristic feature of steam gasification gases in FB is, as a rule, an increased content of CO_2, reaching 28.3% for coal and 25–32% for biomass [11–14] and high hydrogen content (up to 53–66%). Such gases cannot be used for chemical production, but are suitable for hydrogen production, because they almost do not require a water gas shift reaction (WGSR), although they need deep purification due to the content of pyrolysis ballast products. There are data on the production of syngas with relatively close concentrations of H_2 and CO (47 and 38%) at a low content of CO_2 (3.3%) [2].

In this work the equilibrium composition of the reaction products was calculated by the entropy maximization method (EMM) using "restricted equilibria". However, in its pure form, the EMM method, as well as its analogue, the Gibbs energy minimization method, is not suitable for predicting the composition of syngas in a low-temperature FB reactor [15]. This is due to the overly brief gas residence time, which is 2–3 orders of magnitude less than necessary [16]. As a result of such calculations, the content of CO_2, CH_4, and C_2H_4 is usually far from their experimental equivalents [17]. Even in entrained-flow gasifiers at relatively high temperatures (up to 1200 °C), syngas composition can differ markedly from the equilibrium composition, as determined by the WGSR equilibrium constant [18].

Models with "restricted equilibria" allow for the implementation of user-defined constraints. A similar approach is commonly used in modeling in Aspen Plus [19]. Bed gasifiers are also modeled using a multi-zone model based on non-stoichiometric equilibrium models and a redistribution coefficient with a bypass of pyrolysis products through the oxidation zone [20]. According to this approach, only some of the gasification reactions are in equilibrium. At the same time, exact energy balances are achieved only if the experimental gas composition is used as an input parameter for modeling [19].

The research [21] was completed via a study of the influence on the equilibrium of additional parameters such as the quantity of steam, the pressure or the kind of biomass using the Gibbs energy minimization method. In [22], a one-dimensional unsteady state model is developed for simulation of biomass gasification in a bubbling fluidized bed. The effect of biomass feeding position is investigated, and the performance of a reactor under non-isothermal conditions is compared with its performance under isothermal operation. A comprehensive process model is proposed to simulate the steam gasification of biomass in a bubbling fluidized bed reactor using the Aspen Plus simulator [23]. In this work, it was found that the steam-to-biomass ratio is directly proportional to an increase in the content of hydrogen and carbon monoxide, while gas yield and carbon conversion efficiency enhance significantly with increasing temperature. In [24] researchers investigate the fluidized bed gasification of several pure and blended feedstock prepared in the form of pellets: oak bark, two bark/wheat straw blends (85/15 and 50/50% wt) and lignin residue remaining from bioethanol production.

The aim of this work is to study coal steam gasification with various methods of coal in-core treatment in FB using a newly developed thermodynamic calculation method.

The objectives of the research include:

1. Development of a semi-empirical model for calculating steam gasification in FB.
2. Refinement of the steam gasification model based on the experimental results obtained earlier.
3. Carrying out thermodynamic calculational studies of subbituminous coal char steam gasification in the field of technologically justified FB parameters.

2. Methods and Materials

The most common steam gasification technology in FB, combining autothermal and allothermal modes, is a multi-stage multi-section technology with external circulation (Figure 1). Such a multi-vessel technology makes it possible to spatially separate the heating, pyrolysis, and gasification zones by fuel and gas, while maintaining intensive heat and mass transfer both within the zones and between them [25].

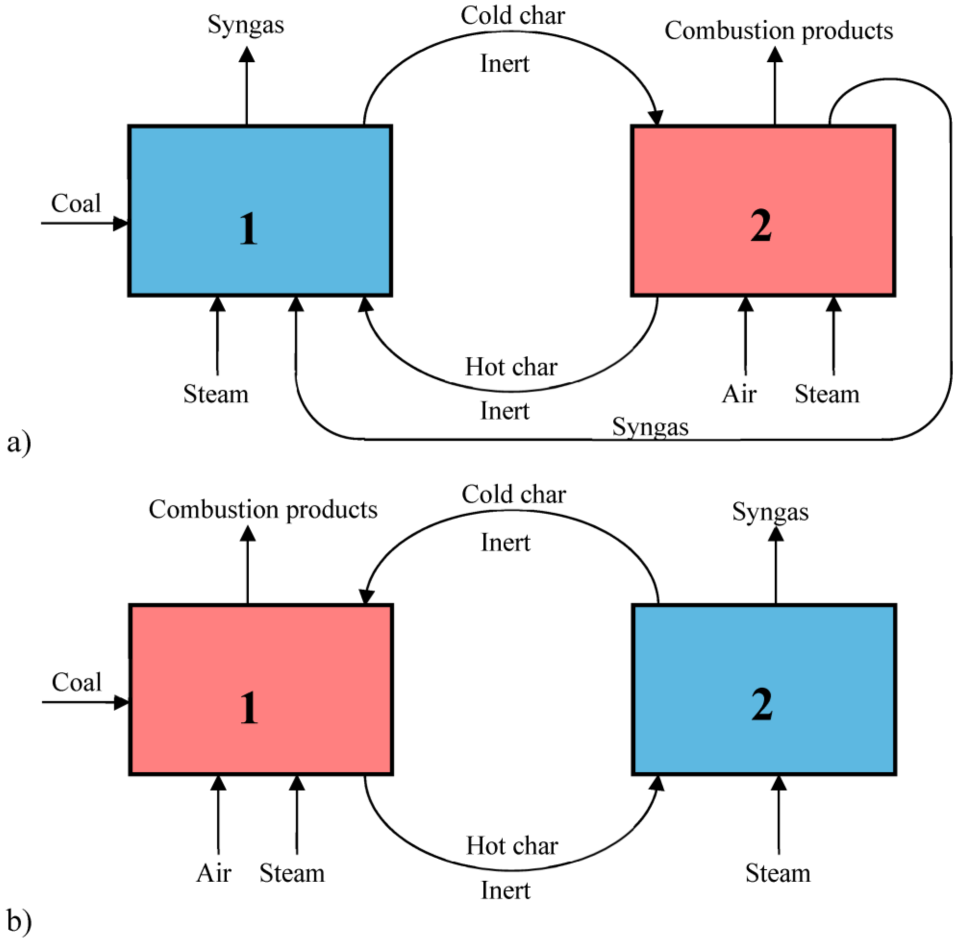

Figure 1. Schemes of media movement in double-vessel gasifiers with external circulation: (**a**) DFB-I; (**b**) DFB-II.

In most cases, a double-vessel FB (DFB) technology is used, usually combining a coal pyrolyzer with BFB or fast FB (FFB) and a gasifier (either an FB char furnace or a circulating FB (CFB)).

Single-vessel FB (SFB) reactors without internal sectioning for the steam gasification of coal can be used under special conditions (an allothermic regime, prepared fuel, catalytic packing, etc.) [26]. Exploratory studies of autothermal SFBs with steam–oxygen- and steam–air-blown processes are ongoing [27,28]. However, the use of single-vessel gasifiers is more developed in entrained-flow high-temperature steam-oxygen-blown technologies [29], or in special gasifiers with low-temperature plasma [30–32].

In some cases, gasification is carried out in one vessel via a two-section FB (SDFB) and a three-section FB (STFB) with internal sectioning and internal circulation (Figure 2). Single-vessel gasifiers with internal sectioning SDFB and STFB allow, as do multi-vessel gasifiers, to separate the heating, pyrolysis, and gasification zones and control the operation of the gasifier in autothermal mode [1,33,34].

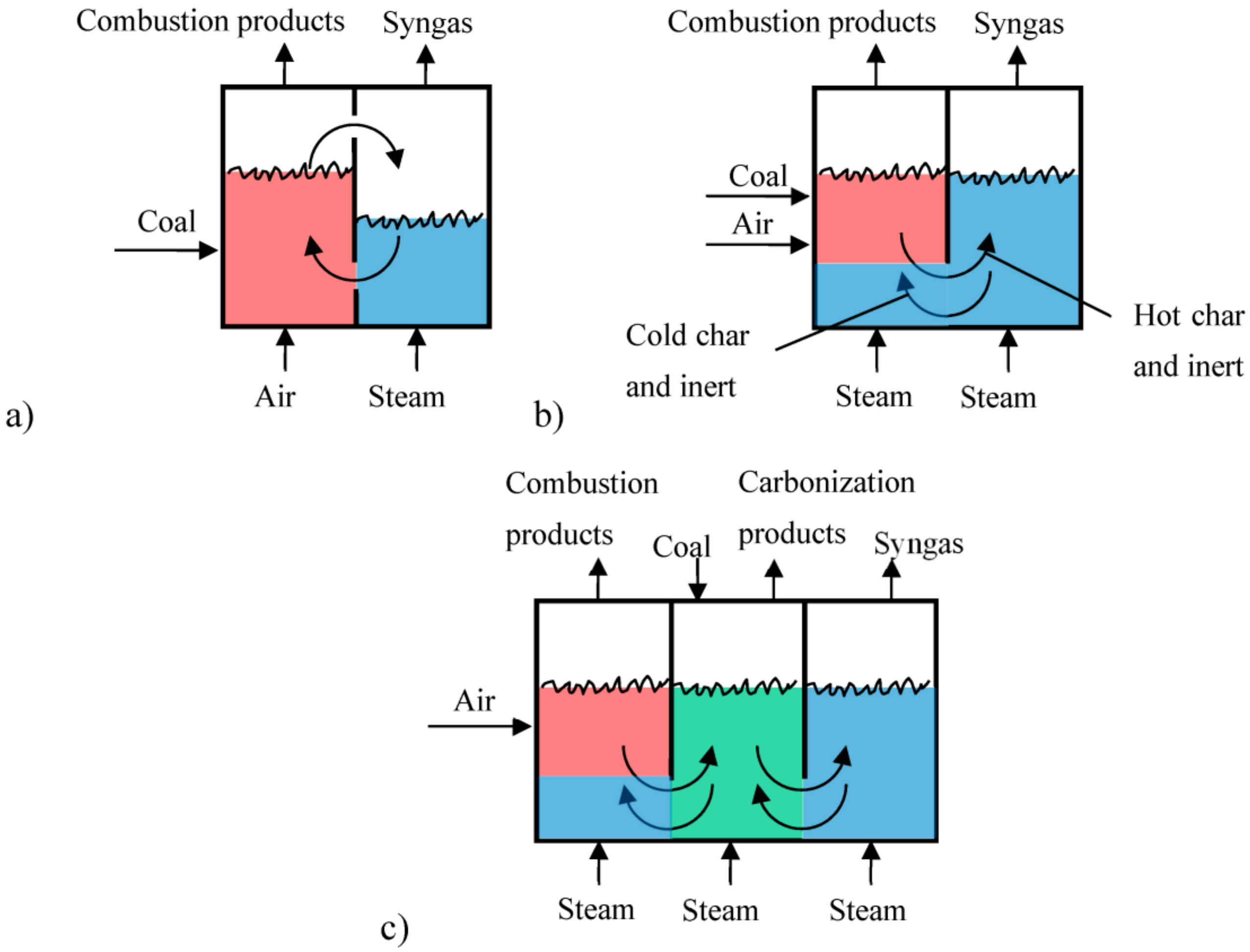

Figure 2. Schemes of media movement in single-vessel gasifiers with internal sectioning: (**a**) SDFB-I; (**b**) SDFB-II; (**c**) STFB.

Multi-section gasifiers operate according to one of two schemes. In Group I gasifiers, syngas is withdrawn from the same gasifier into which all initial reagents (fuel, oxidizer, etc.) are supplied, as is the case in single-vessel gasifiers without internal sectioning. A typical example is the DFB-I and TFB-I gasifiers [2,27,28,31,32,35], where raw coal is gasified. In these, the selection of syngas output from the pyrolysis section, which is supplied with coal, steam, and heated ash (pos. 4 of Table 1) or heated char and heated gas (pos. 5 of Table 1), is carried out. In such gasifiers, the syngas consists of the products of fresh coal and char steam pyrolysis.

Table 1. Steam gasification performance in a fluidized bed and in other systems.

No.	**Gasifier**	**Fuel**	**Reagent**		**P, MPa**	**T, °C**	**Syngas Composition**				**Q^d, MJ/m^3**	**Ref**
			Section 1	**Section 2**			**H_2**	**CO**	**CO_2**	**CH_4**		
1	DFB–II, allothermal, 2 vessels, lab scale	Brown coal	Pyrolysis gas coal	Steam	4	742/790	57.5	19.8	20.8	1.9	12.9 (10.6 (gas 1)	[2]
2	DFB–II, allothermal, lab scale	Brown coal	Steam coal	Pyrolysis gas /steam	4	660/666	67.1	3	28.3	1.6	9.58	[2]
3	"Cogas", TFB–II, 5 vessels, autothermal, pilot scale	Bituminous coal subbitumious coal	Generator gas coal	Steam (Section 2) air (Section 3)	0.1	300–800 800 800–900	49.5	32.5	15.6	0	9.44	[2]

Table 1. *Cont.*

No.	Gasifier	Fuel	Reagent		P, MPa	T, °C	Syngas Composition				Q^d, MJ/m^3	Ref
			Section 1	Section 2			H_2	CO	CO_2	CH_4		
4	Agglomerating, DFB-I, autothermal, 2 vessels, pilot scale	Bituminous coal	Steam coal	Air	0.8	850–930 1100	47.9–66.2	0–38.6	3.3–28.2	1.6–1.9	up to 10	[2]
5	"Westinghouse", TFB-I, 2 vessels, 3 sections, autothermal, pilot scale	Coal	Generator gas + coal (Section 1) generator gas + char (Section 2)	Steam/air (3rd section, vessel 2)	1.1–1.7	700–900 (vessel1) 1000–1100 (vessel 2)	14.4	19.2	9.4	2.8	5.2 (vessel 1)	[2]
6	DFB-II, 2 vessels, allothermal, catalytic (Na(OH)$_2$), lab scale	Coal	N_2, Ar coal	Steam	0.1	700	57	8	32	3	-	[36]
						800	56	10	30	3		
						900	55	18	25	3		
7	DFB-II, 2 vessels, allothermal, lab scale	Coal D	Steam coal	Steam	0.1	750	61.2	14.7	15.6	4.7	-	[5]
						850	58.7	16.2	17.1	8.1		
						950	57.8	19	19.4	2.9		
		SS				750	61	16	12	2.1		
						850	62.5	15	10.2	2.4		
						950	60	19.1	12.9	3.7		
8	SFB-I, 1 vessel, autothermal, pilot scale	Anthracite	Steam/O_2 coal		2.5	995	38.49	26.35	23.6	4.89	-	[27]
9	SFB-I, 1 vessel, autothermal, pilot scale	Coal	Steam/air coal		0.1	950	15–20	15–20	10–12	1–2	-	[28]
10	Fixed bed, 2 vessels, allothermal, lab scale	Bituminous coal	Pyrolysis gas coal	Steam	0.1	950	59.6	22.4	16.00	1.33	-	[3]
						1000	52.5	37.6	8.18	1.19		
						1100	52.9	39.6	5.3	0.77		
11	Plasma gasifier, lab scale	Brown coal	Steam coal		-	2427–3177	46.8–51	39.3–46	0	0	-	[35]
12	Plasma gasifier, lab scale	Bituminous coal	Steam/air air coal		-	3077–3577	17.0–61.2	21.5–45.8	0	0	-	[30]
						2417–2577	16.8–17.9	32.4–38.1				
13	Microwave, plasma gasifier, pilot scale	Brown coal	Steam coal		-	1640	39.8	32	18.2	0	-	[31]
14	Microwave plasma gasifier lab scale	Brown coal	Steam/air coal		-	5727	36–49	19–24	24–46	0	-	[32]
15	TFB-II, 1 vessel, 3 sections, autothermal lab scale	Bituminous coal	Steam coal (Section 1)	steam/air кокс (Section 2) steam char (Section 3)	0.1	925–950 *	58.9–75.3	13.2–29.6	6.9–14.7	0–4.5	9.7–11.5	[33]
		Semicoke	Steam semicoke (Section 1)	steam/air semicoke (Section 2) steam semicoke (Section 3)	0.1	925–950 **	47.5–48.6	47.1–48.8	1.8–4.7	0.7–0.8	11.7	

Table 1. *Cont.*

No.	Gasifier	Fuel	Reagent		P, MPa	T, °C	Syngas Composition				Q^d, MJ/m^3	Ref
			Section 1	Section 2			H_2	CO	CO_2	CH_4		
16	DFB-II, 1 vessel, 2 sections, autothermal lab scale	Bituminous coal	Steam/air coal (Section 1)	Steam char (Section 2)	0.1	700–1000 ***	22.2–42.8	15.9–36.1	11.9–22.1	0.4–4.1	9.0–10.4	[34]
17	Fixed bed, 1 vessel, Allothermal, lab scale	Bituminous coal	Steam coal	-	~0.1	900–1200	28–58	19–29	42–17	10–1	220–230 kJ/mol	[37]

*—dry gas, in wet gas H_2O = 9.1–13.2. **—dry gas, in wet gas H_2O = 15.8–18.3. ***—wet gas H_2O = 8.5–35.5.

In group II gasifiers (DFB-II, TFB-II), syngas is withdrawn from the section into which steam, and heated char are fed, while coal is fed into the pyrolyzer for carbonization and heating. In allothermic processes (pos. 1 and 2 from Table 1), heating in the pyrolyzer is carried out with steam, syngas, and helium (in a built-in heat exchanger) [2]. In autothermal schemes, heating is performed with burning volatiles, part of the raw coal and char.

Group I gasifiers produce syngas saturated with hydrocarbons with a higher heating value (about 12 MJ/m^3). Group II gasifiers produce somewhat leaner (9–10 MJ/m^3) and purer syngas (with a lower content of hydrocarbons).

2.1. Experiment

To carry out the planned studies, we used data obtained earlier in two previously developed [33,34] single-vessel FB gasifiers with two and three sections (SDFB-II and STFB-II). The sections are interconnected by internal flows through which the inert material circulates, while heat and fuel particles are transferred throughout the volume of the reaction space. For modeling, steam gasification modes were selected for four different cases of thermochemical in-core treatment of coal, carried out at different temperatures and steam flow rates.

The work of the sections is based on the general properties of FB, of which the main property is their representation as ideal mixing reactors in the solid phase and ideal displacement in the gas phase [38].

The fuel used was subbituminous Borodinskiy coal and semicoke from Borodinskiy coal (Table 2): the particle size distribution was typical for bubble fluidization, with a particle size of 1–1.5 mm. As an inert layer material, a well-flowing corundum with a density of 3900 kg/m^3 and average particle sizes of 0.32 and 0.5 mm was used. Such materials, belonging to group B according to the Geldart classification, form a stationary BFB when blown at relatively low speeds (<2–3 m/s). The high density of inert particles made it possible to use sufficiently small fractions in operating conditions without entrainment from the apparatus.

2.1.1. SDFB-II

The SDFB-II plant consists of a vessel and an inner pipe dividing it into combustion and gasification sections (Figure 3). Raw coal is fed into the oxygen zone of the combustion section, where it heats up and releases the bulk of the rapidly flammable volatiles matter. The resulting gases are distilled by an upward flow, and char particles descend into the oxygen-free zone of the gasifier, fluidized by steam and the products of its interaction with char: they then flow into the central pipe of the steam gasification section. The problem of steam overheating to the required temperature of 700–1000 °C, which is unattainable in thermal power plants with indirect/indirect steam heating, is solved in FB by the most efficient method of direct heating of low-potential steam (~200 °C), circulating hot inert material. The removal of ash, together with some of the inert material, is carried out from the upper gasification section. The flow diagram of media in SDFB-II is shown in Figure 3.

Table 2. Ultimate and proximate analysis of Borodinskiy coal, semicoke and ash composition.

Parameter	**Coal**	**Semicoke**	**Ash**	
LHV, MJ/kg	22.676	26.857	Slagging start temperature, °C	950
W^r, %	7.11	2.51	SiO_2, %	46.8
A^r, %	13.39	14.41	Al_2O_3, %	12.9
C^{daf}, %	71.26	90.48	TiO_2, %	0.6
H^{daf}, %	4.88	1.81	Fe_2O_3, %	7.9
N^{daf}, %	1.21	0.97	CaO, %	25.8
O^{daf}, %	22.26	6.74	MgO, %	5
S^{daf}, %	0.39	-	K_2O, %	0.5
V^{daf}, %	48.89	10.46	Na_2O, %	0.5

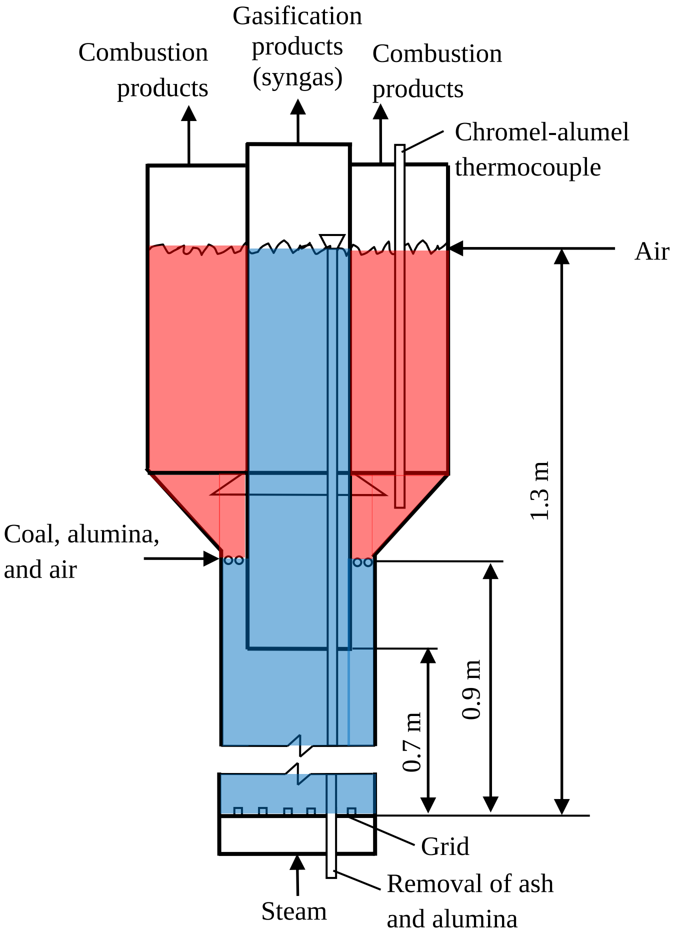

Figure 3. SDFB-II plant diagram.

As shown in Figure 3, at the point of air and coal supply into the gasifier, the newly formed gases are carried away by the upwards gas flow, while the particles of char and ash move downward towards the gas distribution grate. The temperature at the exit from the combustion zone approaches the temperature of the FB (700–1000 °C). This contributes to the development of adverse reactions [39]. Part of the resulting products from side reactions (NO_x, SO_2, CO_2) interact with particles of char and ash according to Equations (1) and (2), [40,41] with the formation of N_2, CO, $CaSO_4$:

$$NO + C = 0.5N_2 + CO \quad (1)$$

$$SO_2 + CaO + 0.5O_2 = CaSO_4 \tag{2}$$

The ash particles, together with the trapped sulfur, are removed through the gasification section. The total gas flow is distributed between the gasification section and the combustion zone in the proportion: $s = (d/D)^2$ in the gasification section and (1-s) in the combustion section.

2.1.2. STFB-II

The STFB-II consists of a vessel and two inner tubes arranged concentrically, one inside the other (Figure 4). The gasifier is divided by these pipes into three sections: central—steam pyrolysis–carbonization; outdoor—steam–air combustion; and an annular gap between them—steam gasification. High superheated steam pyrolysis is a well-known technology widely used to produce activated carbon [42].

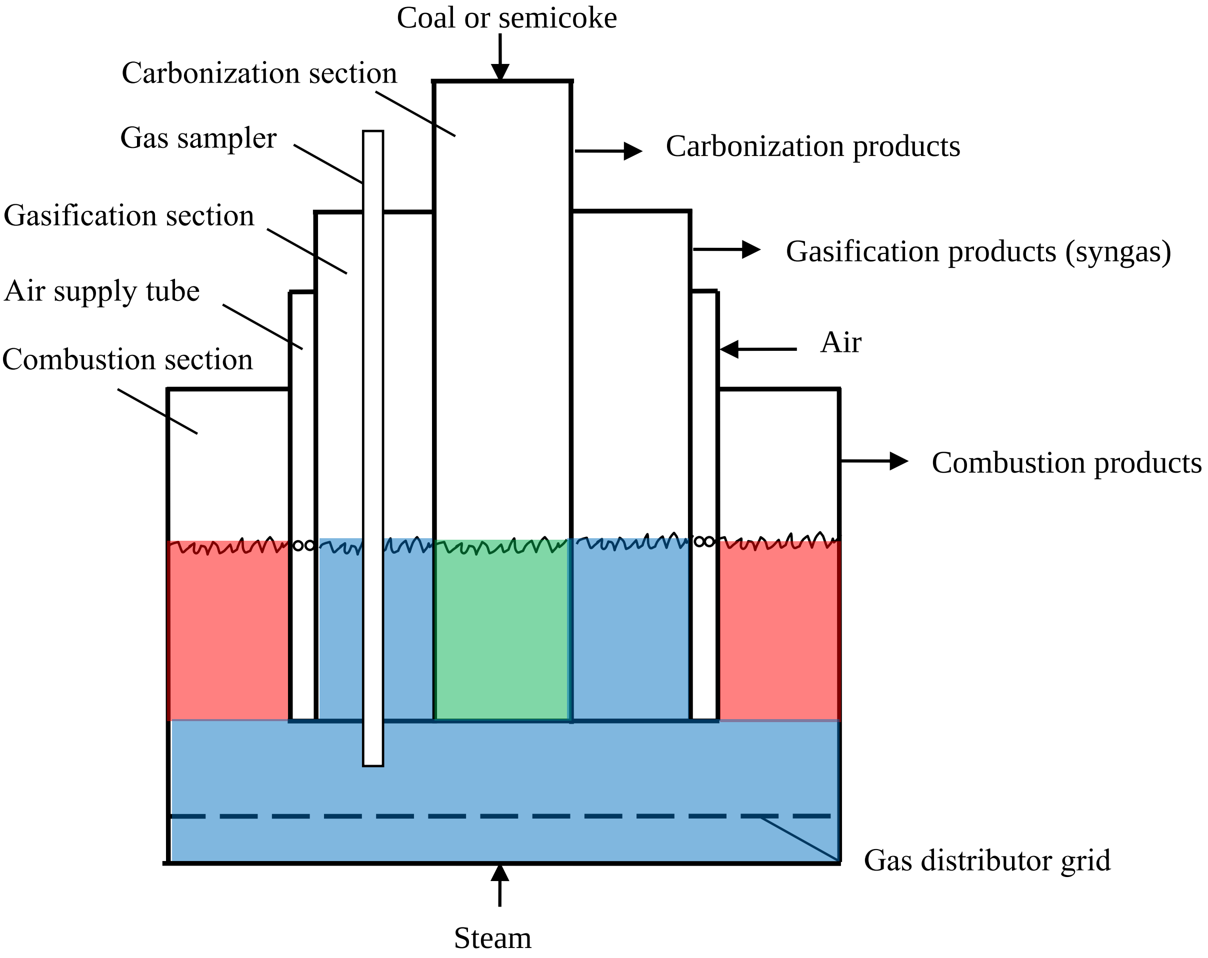

Figure 4. STFB-II gasifier.

The products from each section are removed separately through pipes, while the heat from the combustion zone is carried throughout the gasifier by circulating particles. Raw fuel is supplied to the oxygen-free zone through nozzle, where char with a stable graphite-like carbon structure is formed in the reducing environment. An increase in the reactivity of such a product is mainly due to an increase in the growth of quantitative indicators (the reactive surface of particles during the crushing or opening of internal pores). The char formed in the pyrolysis–carbonization section enters the gasification and combustion sections.

The operating conditions of the gasifiers and the experimental syngas compositions are given in Tables 3–5.

Table 3. Operating conditions for the gasifier.

Parameter	**SDFB-II**	**STFB-II**
Gasifier diameter	0.28 m	0.18 m
Bed height	1.3 m	1.0 m
Bed temperature	7000–1000 °C	925–950 °C
Gasification section diameter	0.134–0.213 m	0.08/0.03 m
Coal mean particle diameter	1×10^{-3} m	1.2×10^{-3} m
Density of coal	1250 kg/m^3	1250 kg/m^3
Coke bed concentration	0.6 kg on 1 kg of mixture	0.12 kg on 1 kg of mixture
Alumina average particle diameter	0.5×10^{-3} m	0.32×10^{-3} m
Alumina density	3900 kg/m^3	3900 kg/m^3
Alumina minimum fluidization velocity	0.294 m/s	0.127 m/s
Air flow rate	30–100 m^3/h	20–30 m^3/h
Steam flow rate	17 kg/h	4.4 kg/h
Steam velocity	0.4 m/s	0.28 m/s

Table 4. Investigation program.

Parameter	**Case 1**	**Case 2**	**Case 3**	**Case 4**
Gasifier	SDFB-II		STFB-II	
Fuel	Coal			Semicoke
Temperature. °C	700	1000	950	

Table 5. Experimental syngas composition.

Component	**Case 1**	**Case 2**	**Case 3**	**Case 4**
H_2	22.0	42.3	45	39.9
CO	15.9	35.9	17.3	39.7
CO_2	21.9	11.5	10.8	1.4
CH_4	3.9	0.5	0.4	0.7
N_2	0.3	0.1	0	0
H_2O	35.5	8.6	26.5	18.3
O_2	-	-	-	-

In the operating mode at bed temperatures of 700–1000 °C, the superheated steam velocities in the bed near the gas distributor grid were 0.4 m/s in the SDFB-II and 0.28 m/s in the STFB-II. Along the height of the gasifier, the rate of the mixture of steam and gasification products increases due to an increase in the steam conversion products. With complete steam conversion, the gas velocity at the exit from the bed increases by a factor of 2, while the dimensionless velocity $W = u_g/u_{mf}$ reaches 2.72 and 4.4 for SDFB-II and STFB-II, respectively. At the same time, for large particles of coal and semicoke, the gas velocity slightly exceeds the minimum fluidization velocity, due to which there is no accumulation of large particles on the gas distributor grid. Under such hydrodynamic conditions, fuel inert particles are intensively mixed by gas bubbles, creating a high temperature uniformity over the volume of the gasifier sections and a diffusion flow of non-volatile carbon particles from the coal loading are to the ash unloading area in the gasification section.

2.2. Modelling

As shown in the previous section, multiple reaction zones are formed in multi-section gasifiers. Depending on the layout, two to three main zones can be distinguished—the pyrolysis zone, the gasification zone, and the combustion zone; however, these zones do not fully correspond to the corresponding sections. Therefore, a multizone thermodynamic model has been developed to calculate the operation parameters of a multi-sectional gasifier. Similar models apply for single section gasifiers [19]. However, the multi-section gasifier has its own specifics in the form of two or three separate gas outlets (char gas, syngas, and combustion products).

The developed model is based on the following assumptions. The gasifier operates at a steady state at a pressure of 101.13 kPa. The supply air is dry at 25 °C and 101.13 kPa. The ash reaction was not considered. Syngas is an ideal gas consisting of CO, CO_2, H_2, CH_4, H_2O, and N_2. The combustion products consist of CO_2, H_2O, N_2, and O_2. Coal and char contain C, H, N, O, S, H_2O, and ash (inert).

The char composition was determined from the following conditions and assumptions:

(1) in the gasification section, only char is gasified, without raw fuel impurities;

(2) there is no moisture and volatile matter in the char;

(3) the main components of char are fixed carbon and ash.

The equilibrium composition of the reaction products was calculated by the entropy maximization method (EMM) using “restricted equilibria”. A detailed description of the practical implementation of the EMM method and its validation are presented in [35,43].

It follows from the laws of thermodynamics that, in a state of equilibrium, the entropy of an isolated system is maximum. Therefore, the problem of calculating the equilibrium composition can be reduced to finding the coordinates of the conditional maximum entropy. The principle of maximum entropy is valid for any equilibrium system, regardless of the path by which the system has reached equilibrium (according to the second law of thermodynamics):

$$S = \sum\nolimits_{i=1}^{k} S_i^{(p_i)} \cdot n_i + \sum\nolimits_{l=1}^{L} S_l \cdot n_l = \sum\nolimits_{i=1}^{k} \left(S_i^0 - R_0 \ln \frac{R_0 T n_i}{v} \right) \cdot n_i + \sum\nolimits_{l=1}^{L} S_l^0 \cdot n_l, \tag{3}$$

where S—entropy (J/(kg K)); $S_i^{(p_i)}$—entropy of the i-th component of the gas phase (J/(mol K)) at the partial pressure of its equilibrium state $p_i = R_0 T n_i / v$ (Pa); n_i—content of the i-th gaseous component in the system (mol/kg); S_l—entropy of the condensed phase l, which depends only on temperature; v—the specific volume of the system; ${S_i}^0$—standard entropy of the i-th component of the gas phase at temperature T and pressure 0.1 MPa; and R_0—universal gas constant (J/(mol K)).

Determining the parameters of the equilibrium state consists in finding the values of all dependent variables, including the numbers of moles of components and phases at which entropy reaches its maximum. When finding an extremum, additional connections are imposed on the values of the unknown unknowns, reflecting the conditions for the system’s existence: the constancy of the total internal energy (because the system is isolated by condition), the constancy of the mass of chemical elements for a closed system and the condition of general electrical neutrality:

$$-U + \sum\nolimits_{i=1}^{k+L} U_i \cdot n_i = 0; b_j = \sum\nolimits_{i=1}^{k+L} a_{ji} n_i, j = 1, 2, \ldots m; \sum\nolimits_{i=1}^{k} a_{ji} n_i = 0, \tag{4}$$

where U—internal energy (J/(kg K)); U_i—internal energy of the i-th component (J/mol K); a_{ji}—stoichiometric coefficients; m—the number of chemical elements in the system; and b_j—the content of the j-th element in the system.

As a result, to find the composition and properties of an arbitrary composition corresponding to the state of the maximum entropy of a conditionally isolated system, it is necessary to solve a nonlinear system of equations:

$$G_i - R_0 \ln \frac{R_0 T}{v} - R_0 \ln n_i + \sum\nolimits_{j=1}^{m} a_{ji}\lambda_j + a_{ei}\lambda_e = 0, (i = 1, 2, \ldots k); \tag{5}$$

$$\left(G_l + \sum\nolimits_{j=1}^{m} a_{jl}\lambda_j\right) \cdot n_l = 0, (l = 1, 2, \ldots L); \tag{6}$$

$$\sum\nolimits_{i=1}^{k+L} a_{ji} n_i - b_j = 0, (j = 1, 2, \ldots m); \tag{7}$$

$$\sum\nolimits_{i=1}^{k} a_{ei} n_i = 0; \tag{8}$$

$$R_0 T \sum\nolimits_{i=1}^{k} n_i - pv = 0; \tag{9}$$

$$\sum\nolimits_{i=1}^{k+L} U_i n_i - U = 0, \tag{10}$$

where G_i—Gibbs energy of the i-th component (J/(mol K)) and λ_j—the Lagrange multiplier of the j-th component.

The system of Equations (3)–(10) is solved iteratively. The thermochemical and thermodynamic characteristics of individual substances are taken from [44].

However, the reaction of coal with water vapor within the temperature range of 700–1000 °C at atmospheric pressure and in the absence of a catalyst proceeds slowly [36]. The acceleration of the process is possible by organizing preliminary chemothermal preparation (pyrolysis, carbonization), aimed at reducing the content of hydrogen and heteroatoms (nitrogen, oxygen, sulfur) and the formation of new reaction centers, as well as at increasing the specific reaction surface and at increasing the carbon concentration in the feed gasification material. An important factor influencing the degree of devolumization/degassing and the volume and structure of pores is the gas medium. Carrying out pyrolysis in an oxidizing environment is accompanied by a known activation effect, depending on the type of oxidizing agent.

In an atmosphere of atmospheric oxygen with an equivalent ratio greater than one (in the combustion zone), the devolumization process will be accompanied by the external burning of particles without the oxidative study of the opening pores. A system of thin deep pores will be worked out in the steam, and these can have a positive effect on the conversion rate in the gasification section and on the degree of approximation of the syngas parameters to thermodynamic equilibrium.

To consider the kinetic limitations in determining the composition of the syngas, it is necessary to select the weight coefficient of the reactions taking place from the experimental data.

With a relatively high concentration of fixed carbon in the reactor zone, characteristic of FB, the process of its gasification is determined by the competitive course of the following two heterogeneous reactions of water gas:

$$\mathrm{C + H_2O = CO + H_2;\ +117\ kJ/mol;} \tag{11}$$

$$\mathrm{C + 2H_2O = CO_2 + 2H_2;\ +75\ kJ/mol.} \tag{12}$$

Simultaneously with them, the third heterogeneous Boudoard reaction also proceeds:

$$\mathrm{C + CO_2 = 2CO;\ +159\ kJ/mol.} \tag{13}$$

However, this reaction does not participate in the competition due to its secondary role: CO_2 (the reagent of this reaction) appears in the system only after reaction (12) has taken place. These reactions are traditionally used to describe steam gasification [16,17,45].

To assess the competition between the rates of reactions (11) and (12), the coefficient K is used, which shows by how much reaction (12)'s contribution is greater than reaction (11)'s contribution in the format (12)/(11).

The combustion section (in the DFB-II reactor) or carbonization section (in the TFB-II reactor) is supplied with fuel with a known composition, however, the gasification section does not receive raw fuel but the product of its conversion (carbonization)—char, with an unknown composition that varies depending on carbonization conditions (temperature, consumption of carbonizing media (steam and/or air), etc.).

The algorithm for carrying out thermodynamic calculations for developing models and determining the char composition in the gasification section is shown in Figure 5.

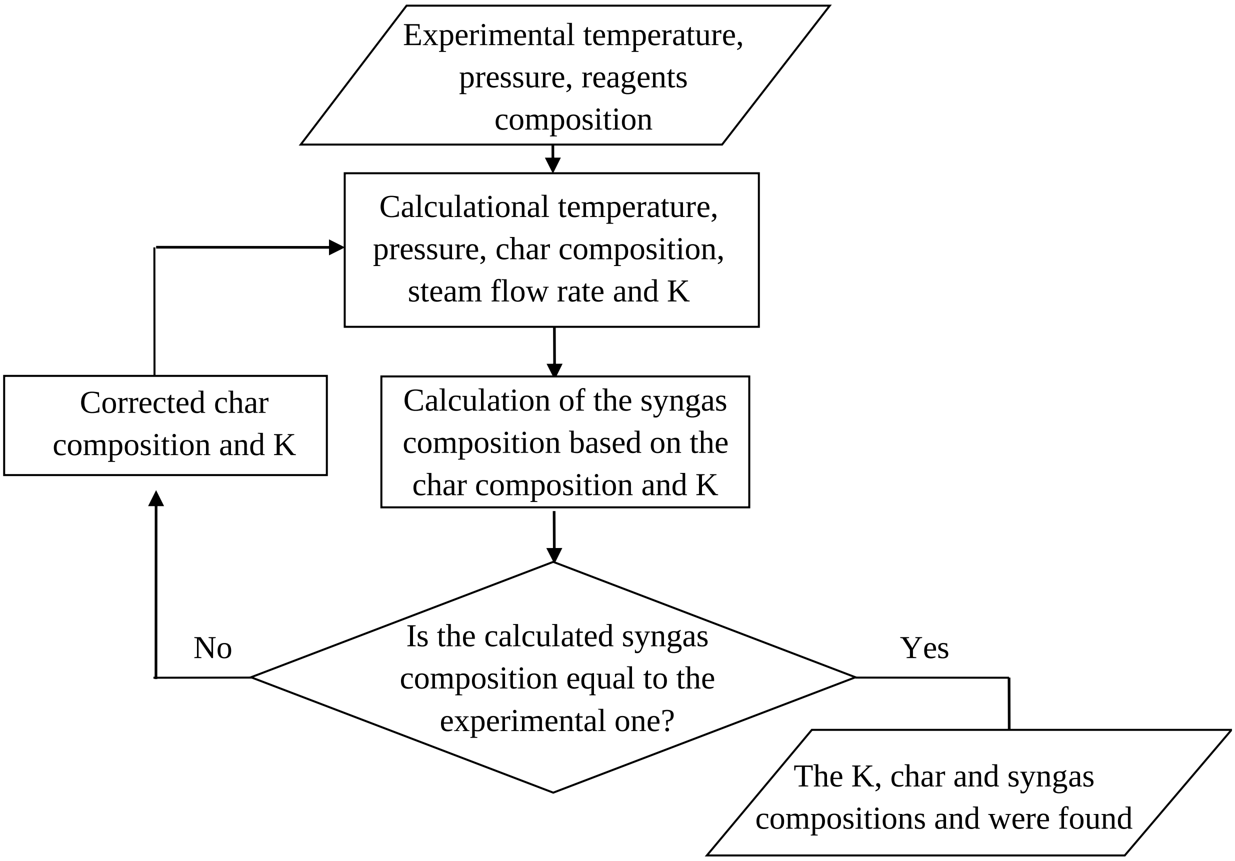

Figure 5. Algorithm for calculating the process of steam gasification in FB.

3. Results and Discussion

3.1. Statistical Evaluation of Results

Based on experimental tests to validate the calculated results obtained, a statistical processing of the data was carried out to confirm the adequacy of the developed model. Figure 6 shows the results of the statistical processing of the concentrations of the main syngas components using the SDFB-II gasifier as an example.

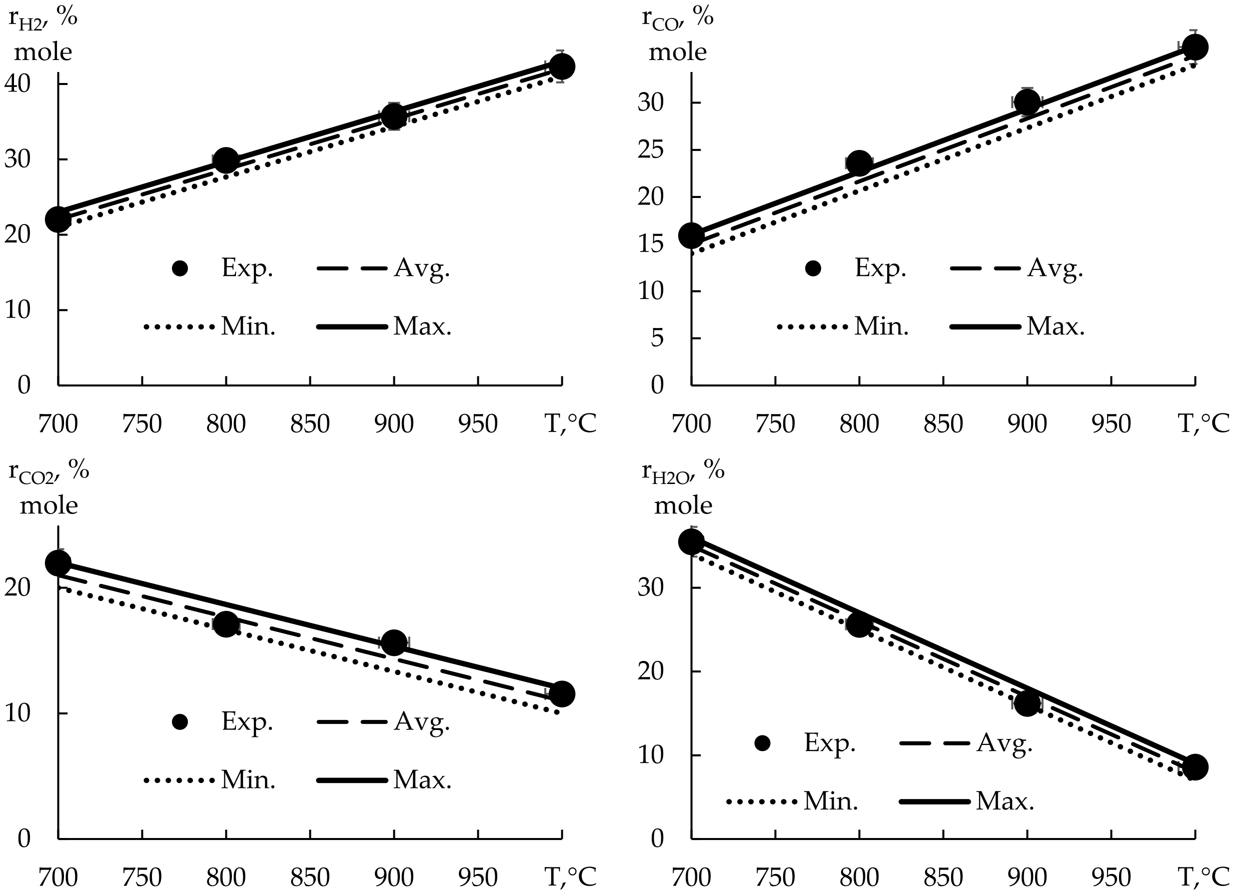

Figure 6. Statistical evaluation of calculation results using experimental data.

As can be seen from Figure 6, the developed model gives results close to the experimental ones. The minimum and maximum values differ from the average by about 1%. The statistical evaluation of the calculation results made it possible to validate the developed model and confirm its satisfactory applicability for solving such problems.

3.2. Dominant Reactions and Their Ratio

The results of multivariate calculations according to the developed algorithm are given in Table 6. Table 6 shows the calculated syngas compositions in three versions:

Table 6. Estimated compositions of syngas.

r, %	**Case 1**				**Case 2**				**Case 3**				**Case 4**			
	A	**B**	**C**	**Exp.**	**A**	**B**	**C**	**Exp.**	**A**	**B**	**C**	**Exp.**	**A**	**B**	**C**	**Exp.**
H_2	47	47	23	22.0	51	49	43	42.3	42	43	41.4	45	47	46	39.8	39.9
CO	29	24	17	15.9	38	46	36	35.9	20	24	24.3	17.3	16	32	39.8	39.7
CO_2	9	13	23	21.9	4	2	12	11.5	9	9	8.5	10.8	7	7	0	1.4
CH_4	3	1	1	3.9	0	0	0	0.49	0	0	0	0.4	0	0	0	0.7
N_2	0	0	0	0.3	0	0	0	0.14	0	0	0	0	0	0	0	0
H_2O	9	15	7	35.5	7	3	9	8.59	29	24	25.7	26.5	16	15	20.3	18.3

A—original version, without taking into account the char composition and coefficient K;

B—variant taking into account the char composition, but without taking into account coefficient K;

C—variant taking into account the char composition and coefficient K (Table 7);

Table 7. Estimated compositions of syngas.

	Case 1	Case 2	Case	Case 4
K	1/2.45	1/1.18	1/1	1/0

Exp.—experimental version.

The convergence of coefficients K from case 1 to cases 2 and 3 indicates a tendency to equalize the degree of completion of the reactions (11) and (12), which occurs due to a change in their rates that occurs with the achievement of parity in case 3 and the subsequent disparity in case 4.

Figure 7 shows that syngas composition (experiment and modelled, as calculated according to version C) generally does not coincide with the equilibrium A and B. An analysis of the ratio of the syngas components found using versions B and C is shown in Figure 6. The experimental (Exp.) and calculated (C) compositions generally do not coincide with the compositions of A and B. The coincidence of B unrestricted and C restricted equilibria is achieved only in case 3, where syngas composition is controlled by WGSR (14):

$$CO + H_2O = CO_2 + H_2; -42{,}9\ kJ/mol. \quad (14)$$

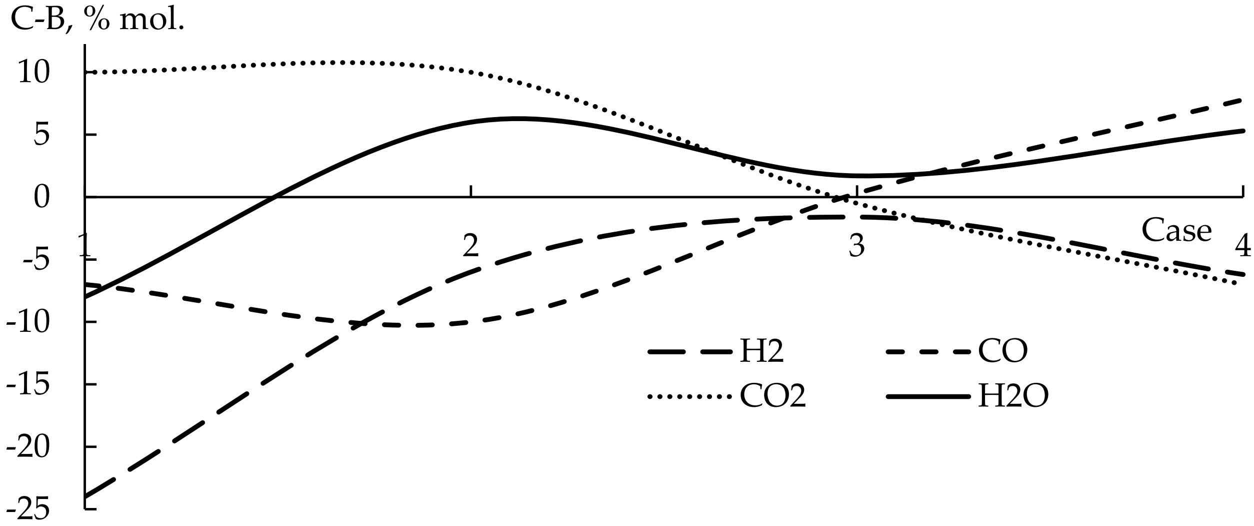

Figure 7. Comparison of calculated results B and C.

In other cases, kinetic restrictions do not allow for the obtaining of syngas with an equilibrium composition. In cases 1 and 2, CO_2 and H_2O are the most abundant in the nonequilibrium mixture, while in case 4, there is an excess of CO and a deficit of CO_2.

In cases 1 (to a greater extent) and 2 (to a lesser extent), the char reactivity is reduced due to oxidative (air) pyrolysis, which occurs in the combustion section. In case 1, the reaction speed is also reduced due to the relatively low temperature of 700 °C. The low reaction rate leads to the dominance of reaction (12), an increase in CO_2, and a decrease in CO. In these cases, the syngas composition obtained by the dominant reaction (12) is first calculated, and then the unreacted carbon reacts with CO_2 according to reaction (13). In case 3, the syngas composition obtained in the experiment and the calculation practically coincide. This indicates the occurrence of reactions (11) and (12) at the same rate, and the achievement of thermodynamic equilibrium at a temperature of 950 °C due to the high char reactivity. In case 2, syngas was obtained at almost the same temperature; however, due to the use of air carbonization, instead of steam, it has an unequal contribution from reactions (11) and (12), which confirms the advantage of steam as a carbonization medium. From the experimental data of case 4, we can see that the syngas H_2 and CO are almost the same, while the CO_2 is negligible, which indicates that reaction (11) proceeds at a much higher rate than reaction (12). This is explained by the greater reactivity of the source fuel (semicoke). The calculation for this case was carried out without considering reaction (12), therefore CO_2 = 0. In case 4, the situation is the reverse to that of cases 1 and 2, since steam carbonization char initially has increased reactivity, and additional steam carbonization in TFB-II further increases it. In this case, reaction (11) dominates so strongly ($CO_2 \approx 0$, H_2 = CO) that reaction (12) can be neglected. Syngas at the outlet again turns out to be non-equilibrium.

As can be seen, the syngas composition calculated from the global equilibrium according to variant A is close to the experimental composition only in case 3. In the other cases, the action of kinetic restrictions does not allow one to obtain the composition of the syngas from the equilibrium of all reactions.

Depending on the competitive course of reactions (11) and (12), the resulting composition approaches one of three gasses:

Gas 1. In the lower temperature range (600–700 °C) with low reaction fuel, reaction (12) is faster than (11). Syngas composition is mainly determined by equation (12), with the characteristic ratio $H_2/CO_2 = 2$.

Gas 2. In the upper temperature range (900–1000 °C) with low-reactivity fuel, reaction (11) is connected to reaction (12), and they begin to proceed at approximately the same rate. Additionally, due to high temperatures, the water gas shift reaction according to reaction (14) is accelerated.

Gas 3. In the upper temperature range with a highly reactive fuel, reaction (12) ceases to determine syngas composition, and the main contribution begins to be made by reaction (11), with the known ratio $H_2/CO = 1$.

The lowest heating value—gas 1—is the most suitable for producing pure hydrogen and reaches the highest concentration of hydrogen. The lowest concentration of hydrogen at the equality $H_2/CO = 1$ will reach the highest heating value—gas 3—which is more suitable for organic syntheses.

Quantitative confirmation of the above explanations can be found in the classical literature on gasification, starting with [45]; however, this describes the results of experiments under special conditions, far removed from those found in industry. The proposed method makes it possible to obtain the calculated syngas composition close enough to the experimental one. The deviation of the calculated data from the experimental data lies in the allowable range of 5–15%. The presented data show the effectiveness of the method of "restricted equilibria" for the predictive study of steam gasification in both low-temperature and high-temperature regimes.

3.3. Char Composition

Char composition was also determined from the above algorithm; however, it does not affect the ratio of the syngas components as much as coefficient K. The char composition (along with the temperature and steam flow rate) is needed to calculate syngas composition. If the temperature and steam flow are determined by the gasifier operating mode, then the reacted char composition is not directly controlled. In our cases, this can be determined only by the algorithm described above, the calculation results for which are shown in Figure 8.

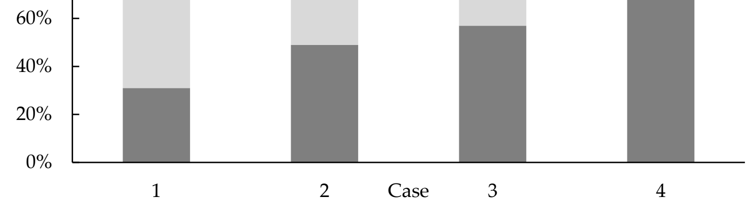

Figure 8. Reacted char composition.

Figure 7 shows that the content of reacted carbon in char increases from case 1 to case 4, and that the ash content decreases without an unambiguous dependence on temperature.

3.4. Temperature Influence

Figure 9 shows the calculation results of the temperature dependences of syngas composition using models describing cases 1–4. The results were obtained using the algorithm (Figure 5) and the obtained char composition (Figure 8). The temperature ranges for cases 1 and 2 were taken from the experiment. For cases 3 and 4, a narrow temperature range of ±50 °C was chosen, since the change in K must be considered over a wide temperature range.

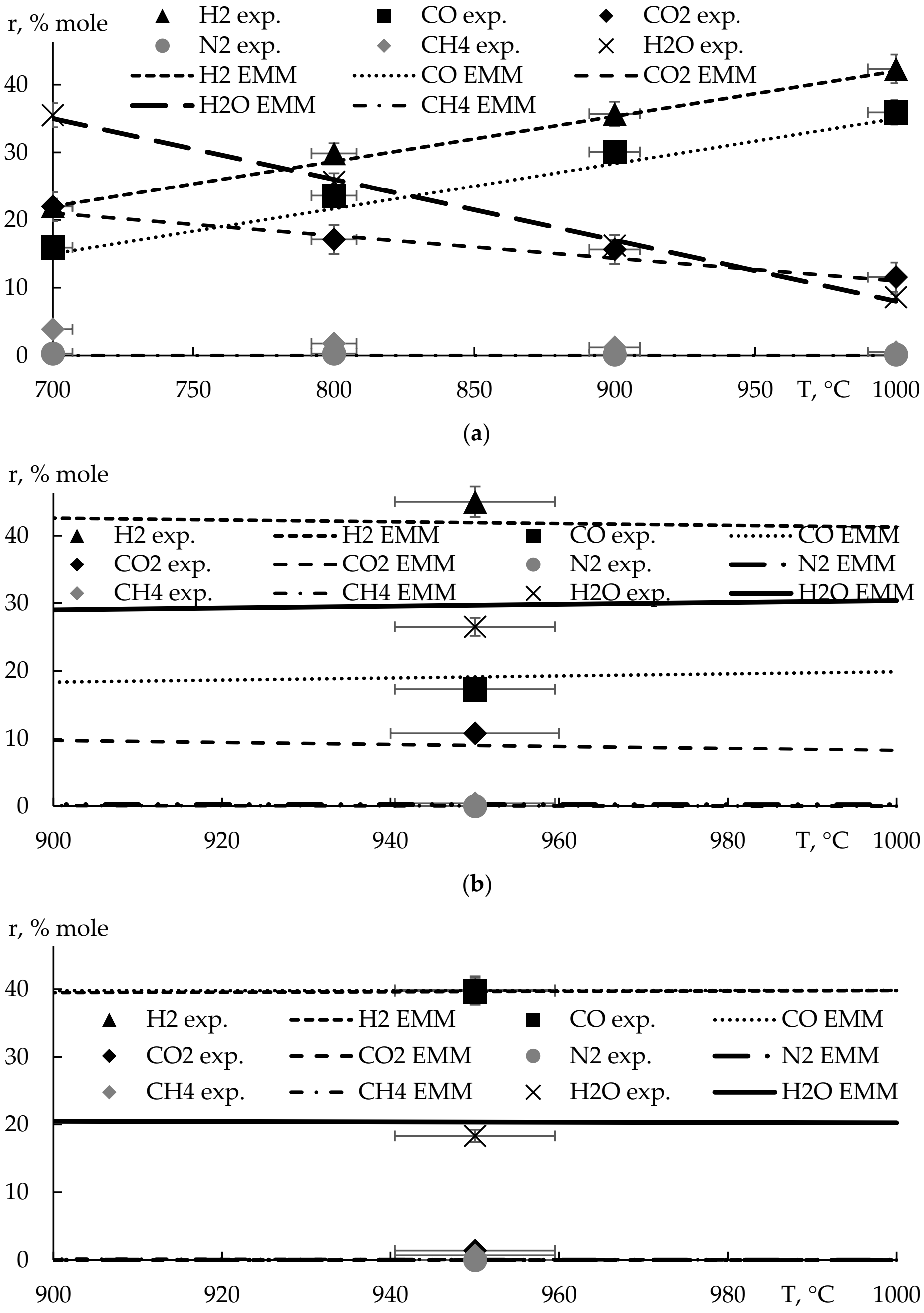

(**a**)

(**b**)

(**c**)

Figure 9. Dependence of syngas composition on temperature in the case of: (**a**) 1 and 2; (**b**) 3; (**c**) 4.

Figure 8 shows the results obtained for SDFB-II. A change in temperature from 700 °C (case 1) to 1000 °C (case 2), which creates differences in the composition and char reactivity, causes a change in the contribution of reactions (12) and (11) from 2.45/1 for case 1 to 1.18/1 for case 2. In the interval between 700 and 1000 °C, the weighting factors change in accordance with Table 8. To obtain these, additional experimental data from [34] were used. Thermodynamic analysis showed that, because of changes to the method of fuel preparation and to the increase of its reactivity at 950 °C, it was possible to achieve an equilibrium syngas composition of the gas 3 type in case 3. In case 2, however, equilibrium was not achieved, even at 1000 °C.

Table 8. Coefficient K for SDFB-II at different temperatures.

	Temperature, °C			
	700	**800**	**900**	**1000**
K	2.45/1	2.02/1	1.61/1	1.18/1

Such a monotonic convergence of coefficients K indicates a tendency to equalize the degree of completion of reactions (11) and (12), which occurs due to the equalization of their rates with increasing temperature. However, as noted above, the equalization of the rates of reactions (11) and (12) in case 2 is not achieved.

Such a redistribution with an increase in temperature by 300 °C causes a doubling of the concentrations of the syngas components: H_2 and CO—towards an increase, and CO_2—towards a decrease. A similar nature of the change in the composition of syngas with temperature is often observed in experimental studies of the steam reforming of coal and biomass in a fluidized bed [1,34]

With a deeper preparation of fuel for gasification, performed in cases 3 and 4 (STFB-II), the contribution of reaction (12) continues to decrease to 1 (case 3) and then to zero (case 4). In this case, the sensitivity of syngas composition to temperature drops sharply (almost to zero in case 4).

To determine the temperature limits of the low sensitivity of the steam reforming gas composition to temperatures in the range of 700–1000 °C, additional experimental studies are required.

Most often, the low temperature sensitivity of the steam reforming syngas composition to temperature is encountered at a higher temperature range—such as in entrained-flow steam-oxygen reactors, plasma processes, etc.—which seem to occur in case 4 [29,35]. The presented data show the flexibility and effectiveness of the method for the predictive study of low-temperature steam reforming in the studied regimes.

3.5. Steam Flow Rate Influence

Figure 10 shows the calculation of the wet (r) and dry (r^d) syngas composition, as well as its heat of combustion depending on the dimensionless steam consumption (g_s) kg of steam/kg of fuel (in our case, char). The lower limit of steam flow rate is selected based on the minimum steam flow required to gasify all of the char carbon, so that no free carbon remains in the system. The calculation for determining this steam flow for all cases was carried out according to equilibrium without restrictions (version C, K = 1/1). The maximum steam flow rate on the graphs was obtained by doubling the minimum value. At the same time, it should be considered that char composition and K can vary depending on steam flow rate. For example, the rate of reaction (12) can increase with an increase in steam consumption and, vice versa, decrease with its decrease. The syngas heating value was determined by the formula:

$$Q = \frac{12.63 \cdot r_{CO} + 10.78 \cdot r_{H_2} + 35.83 \cdot r_{CH_4}}{100} \tag{15}$$

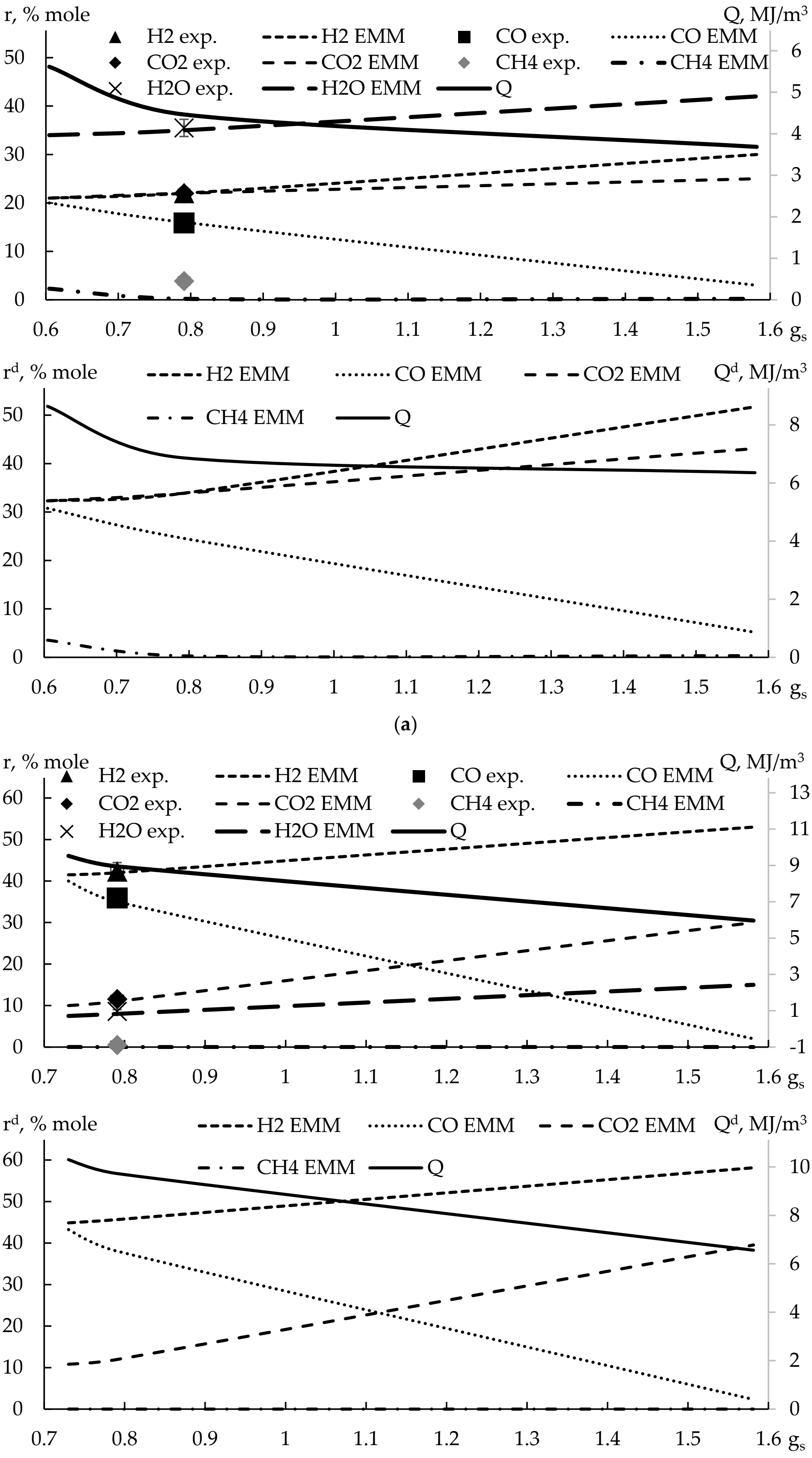

(**a**)

(**b**)

Figure 10. *Cont.*

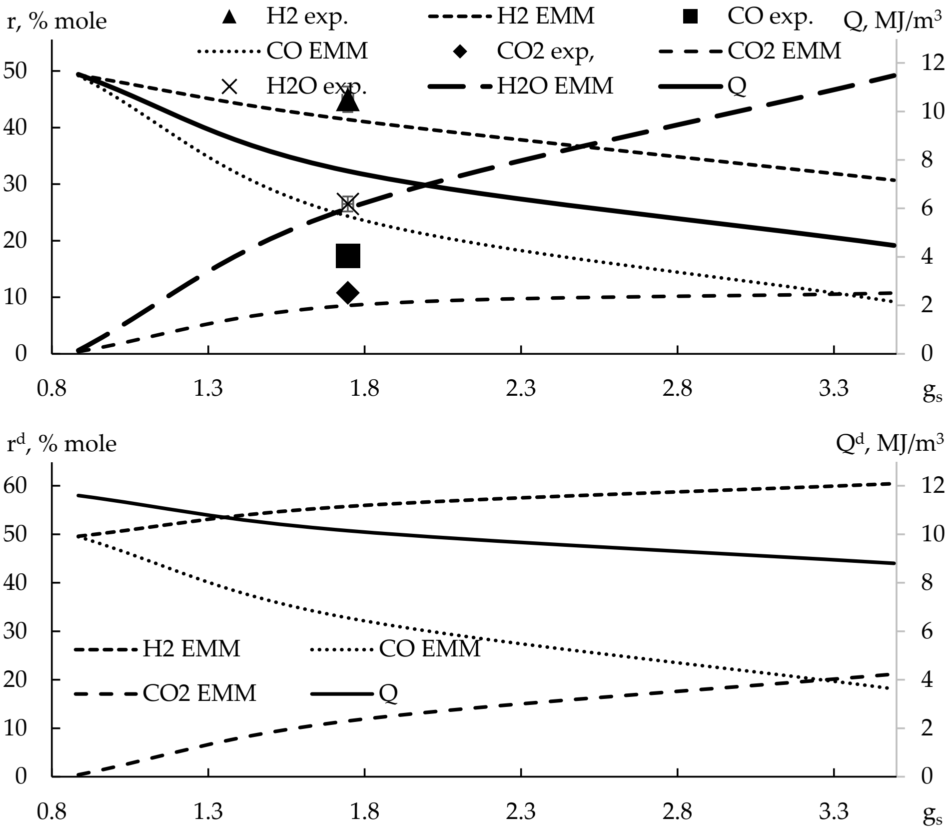

(**c**)

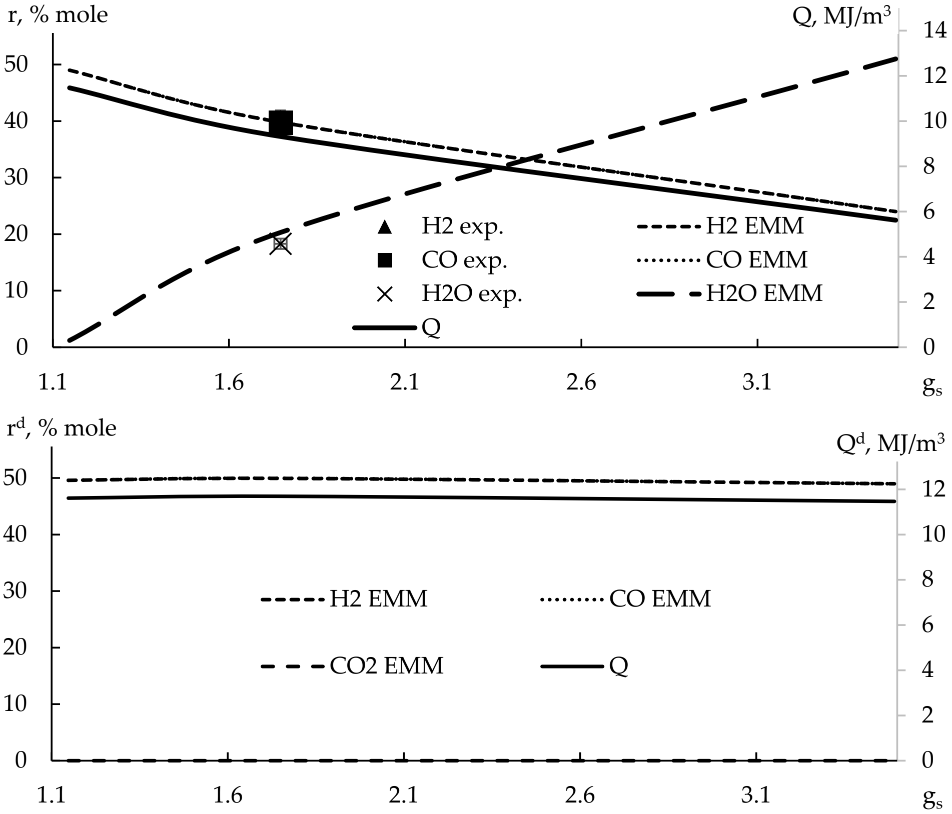

(**d**)

Figure 10. Dependence of wet (r) and dry (r^d) syngas composition on the relative steam consumption in the case of: (**a**) 1; (**b**) 2; (**c**) 3; (**d**) 4.

Figure 9 shows that, with increasing steam consumption, the concentrations of CO_2 and H_2 increase due to reaction (14), while the content of H_2O increases due to the dilution of syngas with steam. This is true in all cases except for case 4, because reaction (14) is impossible due to the absence of CO_2 and reaction (12). The heating value in all cases has its maximum at a minimum steam flow. With an increase in steam consumption, the heating value decreases. This is due to the increased concentration of H_2 and the decreased proportion of CO, given that the heating value of CO is greater than that of H_2. Dependencies of the same kind are also observed in experimental studies, such as in [46]. At the minimum steam flow, syngas composition is close to gas 3, and at the maximum steam flow, to gas 1.

Table 9 compares the obtained results with data from other steam-blown gasifiers. Rows 4–7 show the calculated data of the experimental and optimized modes obtained on the SDFB-II and STFB-II. Optimization was carried out according to the heating value of the syngas. The only parameter that significantly increases the calorific value of syngas in the cases under study is the steam flow rate, namely its reduction (Section 3.4). Therefore, the optimized modes are those in which the steam flow rate is reduced to the minimum required to avoid free carbon in the system.

Table 9. Steam-blown gasifiers.

No.	**Gasifier**	**Fuel**	**g_s, kg/kg of Fuel**	**P, MPa**	**T, °C**	**Dry Syngas Composition**				**Q^d, MJ/m^3**
						H_2	**CO**	**CO_2**	**CH_4**	
1	Entrained-flow [29]	Oil palm residues	1–8.4	0.1	1000	42–55	25–12	14–25	6–5	9.9–9.2
2	Fixed bed [8]	Palm kernel shells	0.85	0.1	850	48.2	28.2	15.9	7.6	11.5
3	Fluidized bed [46]	Wood	0.83–1.2	0.1	840	45.8–48.2	21.1–19.9	19.2–19.4	6.9–5.9	10.1–9.8
					750	38.3–44.3	22.2–17.9	20.7–22	8–6.6	9.8–9.4
			1.2	0.1–0.25		44.3–45	17.9–11.8	22–26.6	6.6–9	9.4–9.6
4	Case 1 (before optimization/after optimization)	Subbituminous coal	0.79/0.61	0.1	700	34/32	25/31	34/32	0.3/3.5	6.9/8.6
5	Case 2 (before optimization/after optimization)	Subbituminous coal	0.79/0.73	0.1	1000	46/45	38/43	12/11	0/0	9.7/10.3
6	Case 3 (before optimization/after optimization)	Subbituminous coal	1.7/0.9	0.1	950	56/50	33/49	1/0	0/0	10.1/11.6
7	Case 4 (before optimization/after optimization)	Semicoke	1.7/1.1	0.1	950	50/50	50/50	0/0	0/0	11.6/11.6

It can be seen from Table 9 that, due to optimization, the heating value of dry syngas increased by 25, 6, and 15% in cases 1, 2, and 3, respectively. In case 4 the heating value remained unchanged, because at K = 0/1 the composition of the syngas does not depend on the steam flow rate. The largest increase in the heating value occurred in case 1 due to a significant increase in the concentration of CH_4, which is undesirable in systems with cold gas cleaning due to its ability to condense. The heating value in the optimized case 3 and in case 4 exceeds the values obtained in the literature, and at the same time does not contain CH_4, as in [46].

Thus, the proposed model allows one to optimize the gasifiers. Sensitivity analysis in such systems can be performed using the matrix decomposition technique [47]. The development of more complex models will require the use of the Statistical and Dynamic System Criteria [48].

3.6. Pressure Influence

The influence of pressure on syngas composition is shown in Figure 11. The pressure range is selected as 0.1–4 MPa, based on the range of operating pressures encountered in the installation with the FB. Pressure can affect the composition of the reacting char and K, but additional experimental studies are needed to evaluate this effect.

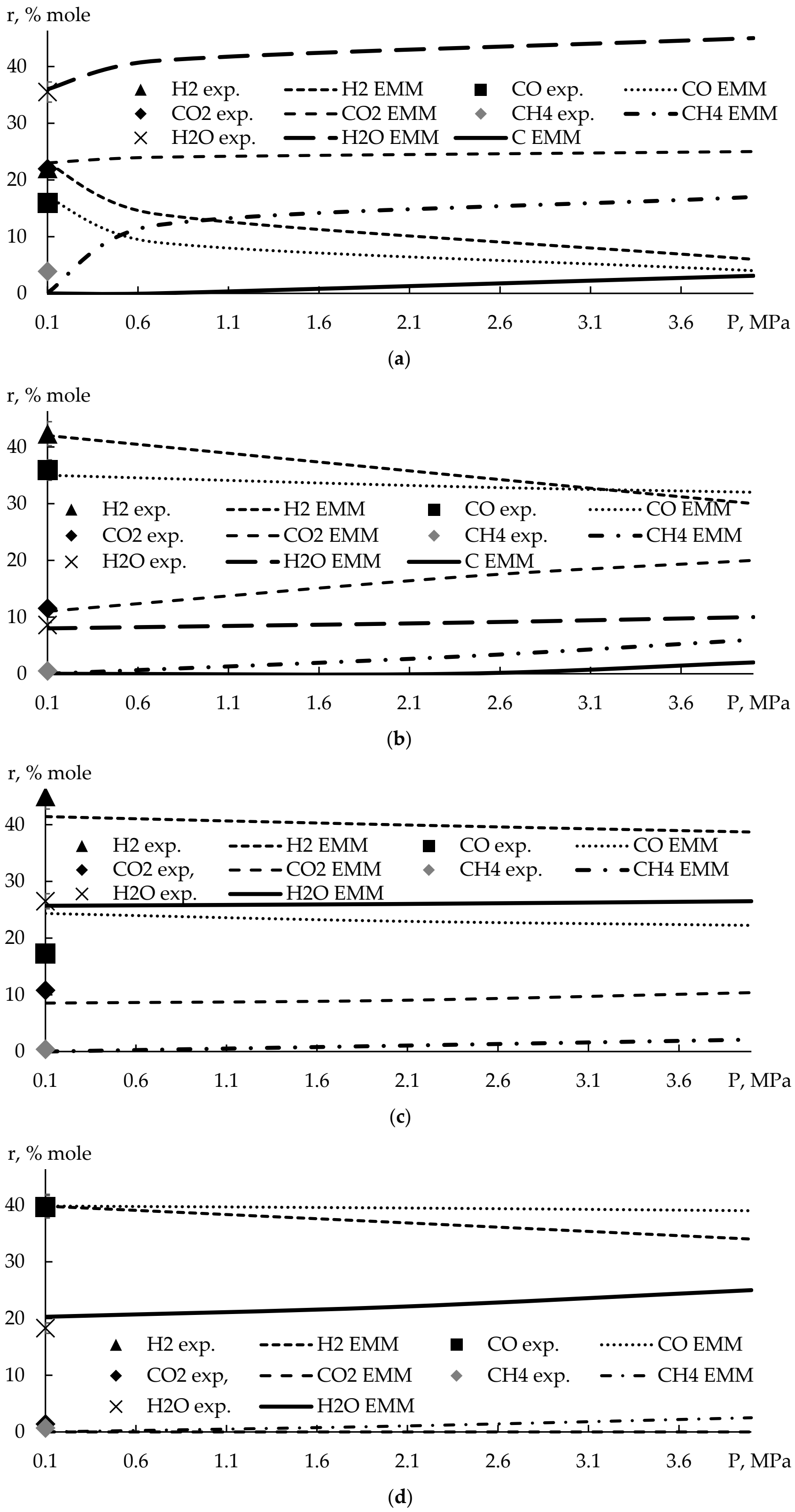

Figure 11. Dependence of syngas composition and heating value on the relative steam flow rate in the case of: (**a**) 1; (**b**) 2; (**c**) 3; (**d**) 4.

Figure 11 shows that in cases 1 and 2, at pressures greater than 0.7 and 2.35 MPa, free carbon begins to be present in the system, which is explained by a shift in the equilibrium of heterogeneous reactions (11)–(13) to the side with a smaller volume (number of moles) according to the Le Chatelier–Brown principle. In case 2, the pressure of the appearance of free carbon in the system is higher, since the temperature is higher; according to the Le Chatelier–Brown principle, the balance of endothermic reactions shifts towards the formation of reagents. In cases 3 and 4, free carbon does not appear in the system in the studied pressure range, as the reactivity of the fuel in these cases is higher. In all cases, the same trend is observed—the proportion of heavy molecules (CH_4, CO_2, H_2O) increases, while the proportion of light molecules (CO and H_2) decreases, something which is also explained by the Le Chatelier–Brown principle. In general, this character of the dependence of syngas composition on pressure in gasifiers with FB is quite characteristic and has been experimentally confirmed [46].

3.7. Comparison with Literature Data

Table 10 shows a comparison of syngas component ratios from the literature data and the performed calculation. In some gasifiers CO or $CO_2 \approx 0$, in this case the table shows "-".

Table 10. Comparison of syngas component ratios.

No.	Gasifier	H_2/CO	H_2/CO_2	CO/CO_2	Q^d, MJ/m^3	Gas Type (from Section 3.1)
1	DFB-II, allothermal, 2 vessels, lab scale [2]	2.9	2.8	1	10.6	2
2	DFB-II, allothermal, lab scale [2]	22.4	2.4	0.1	9.58	1
3	"Cogas", TFB–II, 5 vessls, autothermal, pilot scale [2]	1.5	3.2	2.1	9.44	3
4	Agglomerating, DFB-I, autothermal, 2 vessels, pilot scale [2]	-	14.5	0	10	2
5	"Westinghouse", TFB-I, 2 vessels, 3 sections autothermal, pilot scale [2]	0.75	1.5	2.1	5.2	1
6	DFB-II, 2 vessels, allothermal, catalytic ($Na(OH)_2$), lab scale [36]	7.1	1.7	0.25	7.1	2
7	DFB-II, 2 vessels, allothermal, lab scale [5]	4.2	3.9	0.9	11.2	2

Table 10. *Cont.*

No.	Gasifier	H_2/CO	H_2/CO_2	CO/CO_2	Q^d, MJ/m^3	Gas Type (from Section 3.1)
8	Case 1 (before optimization/after optimization)	1.4/1	1/1	0.7/1	6.8/7.3	2/1
9	Case 2 (before optimization/after optimization)	1.2/1	3.8/4	3.2/4	9.8/10.3	2/3
10	Case 3 (before optimization/after optimization)	1.7/1	56/-	33/-	10.2/11.6	2/3
11	Case 4 (before optimization/after optimization)	1/1	-/-	-/-	11.7/11.7	3/3

As can be seen from Table 10, most of the gasifiers from the literature review produce gas 2 and two of them produce gas 1. This is explained by the low char reactivity, which is prepared from coal in these gasifiers. As a rule, the coal treatment in these gasifiers takes place in an oxidizing atmosphere of air oxygen or steam, which leads to significant differences in the carbonized product (char) reactivity and the syngas composition of char steam-blown gasification. As a result, under the same temperature regime and residence time in the gasification section in cases 2, 3, and 4, syngas was obtained with different degrees of approximation to thermodynamic equilibrium. Oxygen reacts relatively quickly with carbon, so the conversion occurs on the particle surface, reducing its area and reactivity. Therefore, the char conversion in cases 1 and 2 does not reach thermodynamic equilibrium ($K > 1/1$), the syngas tends to gas 2, and in the case of optimization it approaches (but does not reach) gases 1 and 3. The steam reacts slower than oxygen, therefore, it has time to penetrate the pores, react in them, and increase their size, particle area and reactive ability. Therefore, the char conversion in case 3 reaches thermodynamic equilibrium ($K = 1/1$) according to the gas 2 already in the non-optimized mode. Additionally, the conversion of semicoke, which has undergone additional carbonization even before loading into the gasifier, is ultimately observed, again, to be non-equilibrium, but with the dominance of reaction (11), $K = 1/0$, which determines the composition of gas 3.

Based on the results obtained, the following recommendations were made—when designing multi-section and multi-vessel steam-blown gasifiers, the ratio of residence times should be set in favor of increasing the coal residence time in the steam-blown carbonization zone. Structurally, this can be achieved by increasing the volume and/or area of the steam-blown carbonization section (vessel).

4. Conclusions

(1) A new efficient, reliable, and simple method for calculating syngas composition at the gasifier outlet using the EMM method with the “restricted equilibria” approach has been developed. This makes it possible to visually interpret the actual data, clearly determine the limits of applicability of the reactions and confidently predict the linear development of the process in the confidence range of the variation of the system parameters.

(2) The effectiveness of in-core thermochemical fuel treatment in improving the syngas quality by increasing the reactivity of the steam-blown processed fuel was determined. This makes it possible to significantly guide the fast conversion processes in the FB closer to thermodynamic equilibrium and achieve, in a controlled process, the syngas compositions required by the chemical industry, such as gas 3 ($H_2/CO = 1$, $CO_2 = 0$) and gas 1 ($H_2/CO_2 = 2$, $CO = 0$) without resorting to extreme technologies (plasma) or expensive fillers (catalysts). Such a high quality of syngas is achieved even without the use of steam gasification in multi-vessel FBs. Oxygen reacts relatively quickly with carbon, so the conversion occurs on the surface of the particle, reducing its area and reactivity. Steam reacts more slowly than oxygen, so it has time to penetrate the pores, react in them, and increase their size, particle area and reactive ability. The char obtained from semicoke (case 4) had the longest carbonization, which began even before loading into the gasifier, so it has the maximum reactivity and thus makes it possible to obtain gas 3.

(3) Thermodynamic studies of the process of the steam-blown gasification of subbituminous coal char were carried out in the field with technologically justified parameters of a combustion chamber in terms of temperature (700–1000 °C), pressure (0.1–4 MPa) and steam consumption (0.6–1.7 kg/kg of fuel). Increasing the heating value (optimization) is achieved by reducing the steam flow rate to that which was stoichiometrically necessary for the absence of free carbon from the system. The maximum increase in the heating value is achieved in case 1 (10%), and the minimum (no increase) in case 4. Gas 3 is only reached in case 4 before optimization and in all cases after optimization due to oxygen-free conditions for CO_2 formation.

Author Contributions: Conceptualization, L.S. and L.D.; methodology, N.A.; software, N.A.; validation, N.A.; formal analysis, N.A. and A.R.; investigation, N.A. and A.R.; resources, A.D.; data curation, A.R.; writing—original draft preparation, V.T., N.A. and A.R.; writing—review and editing, A.R.; visualization, N.A.; supervision, S.A.; project administration, S.A.; funding acquisition, S.A. All authors have read and agreed to the published version of the manuscript.

Funding: Research funding from the Ministry of Science and Higher Education of the Russian Federation (Ural Federal University Program of Development within the Priority-2030 Program) and the National Natural Science Foundation of China (22278142) is gratefully acknowledged.

Institutional Review Board Statement: Not applicable.

Informed Consent Statement: Not applicable.

Data Availability Statement: Not applicable.

Conflicts of Interest: The authors declare no conflict of interest.

Nomenclature

D	gasifier diameter, m
d	gasification section diameter, m
g_s	dimensionless steam consumption, kg of steam/kg of fuel
P	pressure, Pa
Q	heating value, MJ/m^3
R_0	universal gas constant, J/(mol K)
r	volume concentration, %
S	entropy J/(kg K)
T	temperature, °C
u_g	superficial gas velocity, m/s
u_{mf}	minimum fluidization gas velocity, m/s
BFB	bubbling fluidized bed
CFB	circulating fluidized bed
DFB	double-vessel fluidized bed
EMM	entropy maximization method
FB	fluidized bed
FFB	fast fluidized bed
IGCC	integrated gasification combined cycle
SFB	single-vessel fluidized bed
SDFB	two-section fluidized bed
STFB	three-section fluidized bed
WGSR	water gas shift reaction

References

1. Karl, J.; Pröll, T. Steam gasification of biomass in dual fluidized bed gasifier: A review. *Renew. Sustain. Energy Rev.* **2018**, *98*, 64–78. [CrossRef]
2. Schilling, H.-D.; Bonn, B.; Kraus, U. *Coal Gasification*; Graham and Trotman: London, UK, 1981; p. 175.
3. Wang, D.; Li, S.; He, S.; Gao, L. Coal to substitute natural gas based on combined coal-steam gasification and one-step methanation. *Appl. Energy* **2019**, *240*, 851–859. [CrossRef]

4. Chavan, P.; Datta, S.; Saha, S.; Sahu, G.; Sharma, T. Influence of high ash indian coals in fluidized bed gasification under different operating conditions. *Solid Fuel Chem.* **2012**, *46*, 108–113. [CrossRef]
5. Shevyrev, S.A.; Mazheiko, N.E.; Yakutin, S.K.; Strizhak, P.A. Investigation of characteristics of gas and coke residue for the regime of quasi- and non-stationary steam gasification of coal in a fluidized bed: Part 1. *Energy* **2022**, *251*, 123938. [CrossRef]
6. Aigner, I.; Pfeifer, C.; Hofbauer, H. Co-gasification of coal and wood in a dual fluidized bed gasifier. *Fuel* **2011**, *90*, 2404–2412. [CrossRef]
7. Kern, S.; Pfeifer, C.; Hofbauer, H. Gasification of lignite in a dual fluidized bed gasifier—Influence of bed material particles size and the amount of steam. *Fuel Process. Technol.* **2013**, *111*, 1–13. [CrossRef]
8. Barco-Burgos, J.; Carles-Bruno, J.; Eicker, U.; Saldana-Robles, A.L.; Alcantar-Camarena, V. Hydrogen-rich syngas production from palm kernel shells (PKS) biomass on a downdraft allothermal gasifier using steam as a gasifying agent. *Energy Convers. Manag.* **2021**, *245*, 114592. [CrossRef]
9. Feng, J.; Yan, S.; Zhang, R.; Gu, S.; Qu, X.; Bi, J. Characteristics of Co–Ca catalyzed coal hydrogasification in a mixture of H2 and CO2 atmosphere. *Fuel* **2022**, *324*, 124486. [CrossRef]
10. Li, B.; Lyu, Z.; Zhu, J.; Han, M.; Sun, Z. Study on the operating parameters of the 10 kW SOFC-CHP system with syngas. *Int. J. Coal Sci. Technol.* **2021**, *8*, 500–509. [CrossRef]
11. Antonelli, J.; Lindino, C.A.; Bariccatti, R.A.; Souza, S.N.M.; Lenz, A.M. Lead adsorption and subsequent gasification with Pinus elliottii waste. *Manag. Environ. Qual. Int. J.* **2017**, *28*, 839–850. [CrossRef]
12. Dubinin, A.M.; Shcheklein, S.E. Mini coal-fired CHP plant on the basis of synthesis gas generator (CO+H_2) and electrochemical current generator. *Int. J. Hydrog. Energy* **2017**, *42*, 26048–26058. [CrossRef]
13. Dubinin, A.M.; Tuponogov, V.G.; Kagramanov, Y.A. Air-based coal gasification in a two-chamber gas reactor with circulating fluidized bed. *Therm. Eng.* **2017**, *64*, 46–52. [CrossRef]
14. Valin, S.; Bedel, L.; Guillaudeau, J.; Thiery, S.; Ravel, S. CO_2 as a substitute of steam or inert transport gas in a fluidised bed for biomass gasification. *Fuel* **2016**, *177*, 288–295. [CrossRef]
15. Pletka, R.; Brown, R.C.; Smeenk, J. Indirectly heated biomass gasifcation using a latent heat ballast—1: Experimental evaluations. *Biomass Bioenergy* **2001**, *20*, 297–305. [CrossRef]
16. Murakami, T.; Xu, G.; Suda, T.; Matsuzawa, Y.; Tani, H.; Fujimori, T. Some process fundamentals of biomass gasification in dual fluidized bed. *Fuel* **2007**, *86*, 244–255. [CrossRef]
17. Puig-Arnavat, M.; Bruno, J.C.; Coronas, A. Review and analysis of biomass gasification models. *Renew. Sustain. Energy Rev.* **2010**, *14*, 2841–2851. [CrossRef]
18. Kobayashi, N.; Tanaka, M.; Piao, G.; Kobayashi, J.; Hatano, S.; Itaya, Y.; Mori, S. High temperature air-blown woody biomass gasification model for the estimation of an entrained down-flow gasifier. *Waste Manag.* **2009**, *29*, 245–251. [CrossRef]
19. Biagini, E.; Barontini, F.; Tognotti, L. Development of a bi-equilibrium model for biomass gasification in a downdraft bed reactor. *Bioresour. Technol.* **2016**, *201*, 156–165. [CrossRef]
20. Liao, C.; Summers, M.; Seiser, R.; Cattolica, R.; Herz, R. Simulation of a pilot-scale dual-fluidized-bed gasifier for biomass. *Environ. Prog. Sustain. Energy* **2014**, *33*, 732–736. [CrossRef]
21. Detournay, M.; Hemati, M.; Andreux, R. Biomass steam gasification in fluidized bed of inert or catalytic particles: Comparison between experimental results and thermodynamic equilibrium predictions. *Powder Technol.* **2011**, *208*, 558–567. [CrossRef]
22. Agu, C.E.; Pfeifer, C.; Eikeland, M.; Tokheim, L.-A.; Moldestad, B.M.E. Detailed One-Dimensional Model for Steam-Biomass Gasification in a Bubbling Fluidized Bed. *Energy Fuels* **2019**, *33*, 7385–7397. [CrossRef]
23. Nguyen, N.M.; Alobaid, F.; Epple, B. Process Simulation of Steam Gasification of Torrefied Woodchips in a Bubbling Fluidized Bed Reactor Using Aspen Plus. *Appl. Sci.* **2021**, *11*, 2877. [CrossRef]
24. Valin, S.; Ravel, S.; Pons de Vincent, P.; Thiery, S.; Miller, H.; Defoort, F.; Grateau, M. Fluidised Bed Gasification of Diverse Biomass Feedstocks and S. Blends—An Overall Performance Study. *Energies* **2020**, *13*, 3706. [CrossRef]
25. Leckner, B. Developments in fluidized bed conversion of solid fuels. *Therm. Sci.* **2016**, *20*, S1–S18. [CrossRef]
26. Midilli, A.; Kucuk, H.; Topal, M.E.; Akbulut, U.; Dincer, I. A comprehensive review on hydrogen production from coal gasification: Challenges and Opportunities. *Int. J. Hydrog. Energy* **2021**, *46*, 25385–25412. [CrossRef]
27. Li, G.; Liu, Z.; Liu, F.; Weng, Y.; Ma, S.; Zhang, Y. Thermodynamic analysis and techno-economic assessment of synthetic natural gas production via ash agglomerating fluidized bed gasification using coal as fuel. *Int. J. Hydrog. Energy* **2020**, *45*, 27359–27368. [CrossRef]
28. Datta, S.; Sarkar, P.; Chavan, P.D.; Saha, S.; Sahu, G.; Sinha, A.K.; Saxena, V.K. Agglomeration behavior of high ash Indian coals in fluidized bed gasification pilot plant. *Appl. Therm. Eng.* **2015**, *86*, 222–228. [CrossRef]
29. Ogi, T.; Nakanishi, M.; Fukuda, Y.; Matsumoto, K. Gasification of oil palm residues (empty fruit bunch) in an entrained-flow gasifier. *Fuel* **2013**, *104*, 28–35. [CrossRef]
30. Messerle, V.E.; Ustimenko, A.B.; Lavrichshev, O.A. Comparative study of coal plasma gasification: Simulation and experiment. *Fuel* **2016**, *164*, 172–179. [CrossRef]
31. Uhm, H.S.; Na, Y.H.; Hong, Y.C.; Shin, D.H.; Cho, C.H. Production of hydrogen-rich synthetic gas from low-grade coals by microwave steam-plasmas. *Int. J. Hydrog. Energy* **2014**, *39*, 4351–4355. [CrossRef]
32. Hong, Y.C.; Lee, S.J.; Shin, D.H.; Kim, Y.J.; Lee, B.J.; Cho, S.Y.; Chang, H.S. Syngas production from gasification of brown coal in a microwave torch plasma. *Energy* **2012**, *47*, 36–40. [CrossRef]

33. Dubinin, A.M.; Munts, V.A.; Baskakov, A.P.; Choinzonov, B.L. Gasification of Irsha-Borodino coal in a fluidized-bed reactor. *Solid Fuel Chem.* **1983**, *17*, 117–120.
34. Dubinin, A.M.; Tuponogov, V.G.; Filippov, D.V. Determining maximum capacity of an autothermal fluidized-bed gas generator. *Therm. Eng.* **2009**, *56*, 421–425. [CrossRef]
35. Messerle, V.E.; Ustimenko, A.B.; Lavrichshev, O.A. Plasma coal conversion including mineral mass utilization. *Fuel* **2017**, *203*, 877–883. [CrossRef]
36. Qiu, P.; Du, C.; Liu, L.; Chen, L. Hydrogen and syngas production from catalytic steam gasification of char derived from ion-exchangeable Na- and Ca-loaded coal. *Int. J. Hydrog. Energy* **2018**, *43*, 12034–12048. [CrossRef]
37. Kriengsak, S.N.; Buczynski, R.; Gmurczyk, J.; Gupta, A.K. Hydrogen production by high-temperature steam gasification of biomass and coal. *Environ. Eng. Sci.* **2009**, *26*, 739–744. [CrossRef]
38. Kunii, D.; Levenspiel, O. *Fluidization Engineering*, 2nd ed.; Butterworth-Heinemann: Waltham, MA, USA, 1991; p. 490.
39. Wang, X.; Li, Y.; Zhang, W.; Zhao, J.; Wang, Z. Simultaneous SO_2 and NO removal by pellets made of carbide slag and coal char in a bubbling fluidized-bed reactor. *Process Saf. Environ. Prot.* **2020**, *134*, 83–94. [CrossRef]
40. Pérez-Astray, A.; Adánez-Rubio, I.; Mendiara, T.; Izquierdo, M.; Abad, A.; Gayán, P.; de Diego, L.; García-Labiano, F.; Adánez, J. Comparative study of fuel-N and tar evolution in chemical looping combustion of biomass under both iG-CLC and CLOU modes. *Fuel* **2019**, *236*, 598–607. [CrossRef]
41. Ding, N.; Zhang, C.; Luo, C.; Zheng, Y.; Liu, Z. Effect of hematite addition to $CaSO_4$ oxygen carrier in chemical looping combustion of coal char. *RSC Adv.* **2015**, *5*, 56362–56376. [CrossRef]
42. Mondal, S.; Sinha, K.; Aikat, K.; Halder, G. Adsorption thermodynamics and kinetics of ranitidine hydrochloride onto superheated steam activated carbon derived from mung bean husk. *J. Environ. Chem. Eng.* **2015**, *3*, 187–195. [CrossRef]
43. Gorokhovski, M.; Karpenko, E.I.; Lockwood, F.C.; Messerle, V.E.; Trusov, B.G.; Ustimenko, A.B. Plasma technologies for solid fuels: Experiment and theory. *J. Energy Inst.* **2005**, *78*, 157–171. [CrossRef]
44. Chase, M.W.; Davies, C.A.; Downey, J.R.; Frurip, D.J.; McDonald, R.A.; Syverud, A.N. JANAF thermochemical tables. *J. Phys. Chem. Ref. Data* **1985**, *14* (Suppl. 1), 535.
45. Rambush, N.E. *Modern Gas Producers*; Benn Bros. Ltd.: London, UK, 1923; p. 545.
46. Mayerhofer, M.; Mitsakis, P.P.; Meng, X.; de Jong, W.; Hartmut Spliethoff, H.; Gaderer, M. Influence of pressure; temperature and steam on tar and gas in allothermal fluidized bed gasification. *Fuel* **2012**, *99*, 204–209. [CrossRef]
47. Praks, P.; Lampart, M.; Praksová, R.; Brkić, D.; Kozubek, T.; Najser, J. Selection of Appropriate Symbolic Regression Models Using Statistical and Dynamic System Criteria: Example of Waste Gasification. *Axioms* **2022**, *11*, 463. [CrossRef]
48. Yang, Q.; Peng, X. A Fast Calculation Method for Sensitivity Analysis Using Matrix Decomposition Technique. *Axioms* **2023**, *12*, 179. [CrossRef]